# Impurity in a heteronuclear two-component Bose mixture

G. Bighin,[1,2] A. Burchianti,[3,4] F. Minardi,[3,4,5] and T. Macrì[6]

[1]*IST Austria (Institute of Science and Technology Austria), Am Campus 1, 3400 Klosterneuburg, Austria*
[2]*Institut für Theoretische Physik, Universität Heidelberg, Philosophenweg 19, D-69120 Heidelberg, Germany*
[3]*CNR-INO, Istituto Nazionale di Ottica, 50019 Sesto Fiorentino, Italy*
[4]*LENS and Dipartimento di Fisica e Astronomia, Università di Firenze, 50019 Sesto Fiorentino, Italy*
[5]*Dipartimento di Fisica e Astronomia, Università di Bologna, 40127 Bologna, Italy*
[6]*Departamento de Física Teórica e Experimental, and International Institute of Physics, Universidade Federal do Rio Grande do Norte, Campus Universitário, Lagoa Nova, Natal-RN 59078-970, Brazil*

(Received 21 September 2021; accepted 28 June 2022; published 4 August 2022)

We study the fate of an impurity in an ultracold heteronuclear Bose mixture, focusing on the experimentally relevant case of a $^{41}$K - $^{87}$Rb mixture, with the impurity in a $^{41}$K hyperfine state. Our paper provides a comprehensive description of an impurity in a BEC mixture with contact interactions across its phase diagram. We present results for the miscible and immiscible regimes, as well as for the impurity in a self-bound quantum droplet. Here, varying the interactions, we find exotic states where the impurity localizes either at the center or at the surface of the droplet.

DOI: 10.1103/PhysRevA.106.023301

## I. INTRODUCTION

The problem of a mobile impurity hosted in—and interacting with—a reservoir is a paradigm of many-body quantum theory [1]. In general, interactions alter the properties of the impurity, starting from its inertia, in a way that critically depends on the excitation spectrum of the reservoir. Early on, this problem appeared when considering a single electron immersed in the environment of the ion lattice vibrations [2–5], now known as a polaron, more specifically a Bose polaron, to indicate that the environment is composed of bosonic modes, the lattice phonons [6], and recently observed in Refs. [7,8]. In the last few years, initial studies have addressed the Bose polaron in a host system composed by two bosonic species, i.e., a Bose mixture [9–13], whose spectrum is much richer than its single-species counterpart. A remarkable property of Bose mixtures is the possibility to form liquidlike self-bound droplets, arising from the interplay of mean-field attraction and beyond-mean-field repulsion [14,15]. Tuning mean-field interactions through a Feshbach resonance, quantum droplets have been observed in a homonuclear spin mixture of $^{39}$K, both in the presence of an external potential [16,17] and in free space [18], as well as in heteronuclear mixtures of $^{41}$K - $^{87}$Rb [19] and $^{23}$Na - $^{87}$Rb [20]. Quantum droplets, arising from the competition between contact and long-range interactions [21], have been also observed in magnetic gases [22–27] and, recently studied for dipolar mixtures [28–31].

In this paper, we provide a comprehensive description of a mobile impurity in a (heteronuclear) Bose mixture of atoms with contact interactions: We calculate the phase diagram of the impurity in a realistic case where, in the proximity of a Feshbach resonance, an external magnetic field controls the interaction strength between the components of the Bose mixture [32]. First, we apply a variational ansatz to compute the impurity spectral function and the impurity energy in the miscible and immiscible regimes. Then, we derive the beyond mean-field correction to the impurity-mixture interaction, which leads to an effective interaction potential for the impurity that supports several bound states localized at the mixture surface. We apply our analysis to a specific atomic mixture and discuss the experimental verification of these yet unobserved surface polarons. Our findings pave the wave for study and the detection of Bose polarons in collisionally stable and long-lived Bose mixtures. We show how the impurity states we find can provide a tool for probing the droplet, whose study is currently hindered by the lack of adequate diagnostics, allowing for the characterization of quantum fluctuations at the single-particle level, while also permitting us to implement a scheme for the thermometry of the self-bound droplet.

## II. THE SYSTEM

Let us consider a two-component, ultracold, interacting Bose-Bose mixture [33]. The strength of the interspecies contact interaction is determined by the parameter $g_{12} = 2\pi\hbar^2 a_{12}/\mu$, where $a_{12}$ is the interspecies scattering length, $\mu = m_1 m_2/(m_1 + m_2)$ is the reduced mass, $m_i$ is the mass of $i$th species bosons. The strength of the intraspecies contact interaction is determined by $g_{ii} = 4\pi\hbar^2 a_{ii}/m_i$, $i = 1, 2$, with $a_{ii}$ the intraspecies scattering length for the $i$th species, so the system can be described by the Hamiltonian

$$\hat{H}_{\rm bb} = \int d^3r \sum_{i=1,2} \hat{\phi}_i^\dagger(\mathbf{r})\left(-\frac{\hbar^2\nabla^2}{2m_i} + \frac{g_{ii}}{2}|\hat{\phi}_i(\mathbf{r})|^2\right)\hat{\phi}_i(\mathbf{r}) + g_{12}\int d^3r |\hat{\phi}_1(\mathbf{r})|^2|\hat{\phi}_2(\mathbf{r})|^2, \quad (1)$$

 

where the $\hat{\phi}_i^\dagger(\mathbf{r})$ [$\hat{\phi}_i(\mathbf{r})$] field operators create (annihilate) a bosonic field excitation at position $\mathbf{r}$ in the $i$th component, respectively. In addition to this, we also consider a third component in the impurity limit, i.e., a third component much more dilute than the other two, so we can neglect intercomponent interactions and describe it in the first quantization formalism via operators describing the impurity position $\hat{\mathbf{R}}$ and momentum $\hat{\mathbf{P}}$. The Hamiltonian describing the impurity motion and the interaction with the other two components reads

$$\hat{H}_{\mathrm{I}} = \frac{\hat{\mathbf{P}}^2}{2m_{\mathrm{I}}} + \sum_{i=1,2} g_{Ii} \int d^3r\, \rho(\mathbf{r})\, |\hat{\phi}_i(\mathbf{r})|^2, \tag{2}$$

where $\rho(\mathbf{r}) = \delta^{(3)}(\mathbf{r} - \hat{\mathbf{R}})$, $m_I$ is the impurity mass, $g_{Ii} = 2\pi\hbar^2 a_{Ii}/\mu_{Ii}$, where $a_{Ii}$ is the scattering length between the impurity and the $i$th component, and $\mu_{Ii} = m_I m_i/(m_I + m_i)$.

## III. FROM THE DENSITY-DENSITY INTERACTION TO THE EFFECTIVE HAMILTONIAN

To describe the miscible phase, we begin by expanding the field operators in the plane-wave basis

$$\hat{\phi}_1(\mathbf{r}) = \frac{1}{\sqrt{V}} \sum_{\mathbf{q}} e^{i\mathbf{q}\cdot\mathbf{r}} \alpha_{\mathbf{q}},$$
$$\hat{\phi}_2(\mathbf{r}) = \frac{1}{\sqrt{V}} \sum_{\mathbf{q}} e^{i\mathbf{q}\cdot\mathbf{r}} \beta_{\mathbf{q}}. \tag{3}$$

Bogoliubov approximation consists of separating the macroscopic occupation of the ground state from the fluctuations,

$$\hat{\alpha}_{\mathbf{k}} = (2\pi)^3 \sqrt{n_1}\delta(\mathbf{k}) + \hat{A}_{\mathbf{k}\neq 0}, \tag{4}$$

subsequently retaining only terms linear in $\hat{A}$, neglecting higher order terms, having introduced $n_i$, the density of the $i$th component. A completely analogous procedure is employed for the $\hat{\beta}_{\mathbf{k}}$ operators. Subsequently, the Bogoliubov transformation brings the bosonic part of the Hamiltonian $H_{\mathrm{bos}}$ in a diagonal form. In the present case, the Bogoliubov transformation is given by a $4 \times 4$ matrix that rotates the creation and annihilation operators for the two species in the following way [33]:

$$\begin{pmatrix} \hat{A}_{\mathbf{k}} \\ \hat{A}^\dagger_{-\mathbf{k}} \\ \hat{B}_{\mathbf{k}} \\ \hat{B}^\dagger_{-\mathbf{k}} \end{pmatrix} = \begin{pmatrix} M^{11}_{\mathbf{k}} & M^{12}_{\mathbf{k}} & M^{13}_{\mathbf{k}} & M^{14}_{\mathbf{k}} \\ M^{21}_{\mathbf{k}} & M^{22}_{\mathbf{k}} & M^{23}_{\mathbf{k}} & M^{24}_{\mathbf{k}} \\ M^{31}_{\mathbf{k}} & M^{32}_{\mathbf{k}} & M^{33}_{\mathbf{k}} & M^{34}_{\mathbf{k}} \\ M^{41}_{\mathbf{k}} & M^{42}_{\mathbf{k}} & M^{43}_{\mathbf{k}} & M^{44}_{\mathbf{k}} \end{pmatrix} \begin{pmatrix} \hat{a}_{\mathbf{k}} \\ \hat{a}^\dagger_{-\mathbf{k}} \\ \hat{b}_{\mathbf{k}} \\ \hat{b}^\dagger_{-\mathbf{k}} \end{pmatrix}. \tag{5}$$

A full derivation of the coefficients of the Bogoliubov transformation for a general heteronuclear mixture considered in the text is a lengthy calculation. We refer the reader to Ref. [33] for the details. In this new basis, as anticipated, the bosonic part of the Hamiltonian is diagonal and reads

$$H_{\mathrm{bos}} = \sum_{\mathbf{k}} \hbar\omega^{(A)}_{\mathbf{k}} \hat{a}^\dagger_{\mathbf{k}} \hat{a}_{\mathbf{k}} + \sum_{\mathbf{k}} \hbar\omega^{(B)}_{\mathbf{k}} \hat{b}^\dagger_{\mathbf{k}} \hat{b}_{\mathbf{k}}, \tag{6}$$

where $\omega^{(i)}_{\mathbf{k}}$ is the effective dispersion relation for the *ith* normal mode and the $\hat{a}^\dagger_{\mathbf{k}}$ ($\hat{b}^\dagger_{\mathbf{k}}$) operator creates a Bogoliubov excitation for the $A$ ($B$) normal mode, respectively [33]. The density-density interaction term describing a first-quantized impurity in a bosonic many-body bath interacting with two different bosonic species is given by

$$\hat{H}_{\mathrm{imp\text{-}bos}} = g_{I1} \sum_{\mathbf{k},\mathbf{q}} \hat{\rho}(\mathbf{q}) \hat{\alpha}^\dagger_{\mathbf{k}-\mathbf{q}} \hat{\alpha}_{\mathbf{k}} + g_{I2} \sum_{\mathbf{k},\mathbf{q}} \hat{\rho}(\mathbf{q}) \hat{\beta}^\dagger_{\mathbf{k}-\mathbf{q}} \hat{\beta}_{\mathbf{k}}, \tag{7}$$

where $\hat{\rho}(\mathbf{q}) = \exp(i\mathbf{q}\cdot\hat{\mathbf{R}})$ is the Fourier transform of the density of an impurity located at position $\hat{\mathbf{R}}$. In the case of Eq. (7), the separation of Eq. (4) gives

$$\hat{H}^{(1)}_{\mathrm{imp\text{-}bos}} = g_{I1}\sqrt{n_1} \sum_{\mathbf{k}\neq 0} e^{i\mathbf{k}\cdot\hat{\mathbf{R}}} (\hat{A}_{\mathbf{k}} + \hat{A}^\dagger_{-\mathbf{k}}), \tag{8}$$
$$+ g_{I2}\sqrt{n_2} \sum_{\mathbf{k}\neq 0} e^{i\mathbf{k}\cdot\hat{\mathbf{R}}} (\hat{B}_{\mathbf{k}} + \hat{B}^\dagger_{-\mathbf{k}}), \tag{9}$$

having neglected higher order terms in $\hat{A}$ and $\hat{B}$ and having omitted a constant factor $n_1 g_{I1} + n_2 g_{I2}$. Finally, after Bogoliubov transformation and some algebra, the interaction term can be rewritten as

$$\hat{H}^{(1)}_{\mathrm{imp\text{-}bos}} = \sum_{\mathbf{k}\neq 0} U_A(\mathbf{k}) e^{i\mathbf{k}\cdot\hat{\mathbf{R}}} (\hat{a}_{\mathbf{k}} + \hat{a}^\dagger_{-\mathbf{k}}), \tag{10}$$
$$+ \sum_{\mathbf{k}\neq 0} U_B(\mathbf{k}) e^{i\mathbf{k}\cdot\hat{\mathbf{R}}} (\hat{b}_{\mathbf{k}} + \hat{b}^\dagger_{-\mathbf{k}}), \tag{11}$$

having introduced the effective potentials:

$$U_A(\mathbf{k}) = g_{I1}\sqrt{n_1}\left(M^{11}_{\mathbf{k}} + M^{21}_{\mathbf{k}}\right) + g_{I2}\sqrt{n_2}\left(M^{31}_{\mathbf{k}} + M^{41}_{\mathbf{k}}\right), \tag{12}$$
$$U_B(\mathbf{k}) = g_{I2}\sqrt{n_2}\left(M^{33}_{\mathbf{k}} + M^{43}_{\mathbf{k}}\right) + g_{I1}\sqrt{n_1}\left(M^{13}_{\mathbf{k}} + M^{23}_{\mathbf{k}}\right). \tag{13}$$

The total Fröhlich-level Hamiltonian is then $\hat{H} = \hat{H}_{\mathrm{bos}} + \hat{H}_{\mathrm{imp}} + \hat{H}^{(1)}_{\mathrm{imp\text{-}bos}}$.

## IV. EXTENDED HAMILTONIAN

We now include the higher-order terms, i.e., terms $\sim\hat{a}^\dagger\hat{a}^\dagger$ and similar couplings, describing the scattering of the impurity off the condensate. It has been shown [34] that these terms are important for an accurate description of the physics of quantum impurities in ultracold gases. We start from Eq. (7) but now we do not discard terms quadratic in the fluctuations fields; this gives rise to the following additional contribution:

$$\hat{H}^{(2)}_{\mathrm{imp\text{-}bos}} = g_{I1} \sum_{\mathbf{k},\mathbf{k}'} \hat{\rho}(\mathbf{k}+\mathbf{k}') \hat{A}^\dagger_{-\mathbf{k}'} \hat{A}_{\mathbf{k}}$$
$$+ g_{I2} \sum_{\mathbf{k},\mathbf{k}'} \hat{\rho}(\mathbf{k}+\mathbf{k}') \hat{B}^\dagger_{-\mathbf{k}'} \hat{B}_{\mathbf{k}}, \tag{14}$$

so after Bogoliubov transformation the interaction term of Eq. (14) can be split as $\hat{H}^{(2)}_{\mathrm{imp\text{-}bos}} = \hat{H}^{(2A)}_{\mathrm{imp\text{-}bos}} + \hat{H}^{(2B)}_{\mathrm{imp\text{-}bos}}$, with

$$\hat{H}^{(2A)}_{\mathrm{imp\text{-}bos}} = g_{I1} \sum_{\mathbf{k},\mathbf{k}'} \hat{\rho}(\mathbf{k}+\mathbf{k}') \left(M^{21}_{\mathbf{k}'} a_{\mathbf{k}'} + M^{22}_{\mathbf{k}'} a^\dagger_{-\mathbf{k}'} + M^{23}_{\mathbf{k}'} b_{\mathbf{k}'} + M^{24}_{\mathbf{k}'} b^\dagger_{-\mathbf{k}'}\right) \left(M^{11}_{\mathbf{k}} a_{\mathbf{k}} + M^{12}_{\mathbf{k}} a^\dagger_{-\mathbf{k}} + M^{13}_{\mathbf{k}} b_{\mathbf{k}} + M^{14}_{\mathbf{k}} b^\dagger_{-\mathbf{k}}\right) \tag{15}$$

and

$$\hat{H}^{(2B)}_{\text{imp-bos}} = g_{I2}\sum_{\mathbf{k},\mathbf{k}'}\hat{\rho}(\mathbf{k}+\mathbf{k}')\big(M^{41}_{\mathbf{k}'}a_{\mathbf{k}'} + M^{42}_{\mathbf{k}'}a^{\dagger}_{-\mathbf{k}'} + M^{43}_{\mathbf{k}'}b_{\mathbf{k}'} + M^{44}_{\mathbf{k}'}b^{\dagger}_{-\mathbf{k}'}\big)\big(M^{31}_{\mathbf{k}}a_{\mathbf{k}} + M^{32}_{\mathbf{k}}a^{\dagger}_{-\mathbf{k}} + M^{33}_{\mathbf{k}}b_{\mathbf{k}} + M^{34}_{\mathbf{k}}b^{\dagger}_{-\mathbf{k}}\big). \tag{16}$$

An alternative way of writing the extended interaction term is in matrix form, with

$$H^{(2A)}_{\text{imp-bos}} = g_{I1}\sum_{\mathbf{k},\mathbf{k}'}\hat{\rho}(\mathbf{k}+\mathbf{k}')\begin{pmatrix}\hat{a}_{\mathbf{k}'}\\ \hat{a}^{\dagger}_{-\mathbf{k}'}\\ \hat{b}_{\mathbf{k}'}\\ \hat{b}^{\dagger}_{-\mathbf{k}'}\end{pmatrix}^{T}\begin{pmatrix}M^{11}_{\mathbf{k}}M^{21}_{\mathbf{k}'} & M^{12}_{\mathbf{k}}M^{21}_{\mathbf{k}'} & M^{13}_{\mathbf{k}}M^{21}_{\mathbf{k}'} & M^{14}_{\mathbf{k}}M^{21}_{\mathbf{k}'}\\ M^{11}_{\mathbf{k}}M^{22}_{\mathbf{k}'} & M^{12}_{\mathbf{k}}M^{22}_{\mathbf{k}'} & M^{13}_{\mathbf{k}}M^{22}_{\mathbf{k}'} & M^{14}_{\mathbf{k}}M^{22}_{\mathbf{k}'}\\ M^{11}_{\mathbf{k}}M^{23}_{\mathbf{k}'} & M^{12}_{\mathbf{k}}M^{23}_{\mathbf{k}'} & M^{13}_{\mathbf{k}}M^{23}_{\mathbf{k}'} & M^{14}_{\mathbf{k}}M^{23}_{\mathbf{k}'}\\ M^{11}_{\mathbf{k}}M^{24}_{\mathbf{k}'} & M^{12}_{\mathbf{k}}M^{24}_{\mathbf{k}'} & M^{13}_{\mathbf{k}}M^{24}_{\mathbf{k}'} & M^{14}_{\mathbf{k}}M^{24}_{\mathbf{k}'}\end{pmatrix}\begin{pmatrix}\hat{a}_{\mathbf{k}}\\ \hat{a}^{\dagger}_{-\mathbf{k}}\\ \hat{b}_{\mathbf{k}}\\ \hat{b}^{\dagger}_{-\mathbf{k}}\end{pmatrix} \tag{17}$$

and

$$H^{(2B)}_{\text{imp-bos}} = g_{I2}\sum_{\mathbf{k},\mathbf{k}'}\hat{\rho}(\mathbf{k}+\mathbf{k}')\begin{pmatrix}\hat{a}_{\mathbf{k}'}\\ \hat{a}^{\dagger}_{-\mathbf{k}'}\\ \hat{b}_{\mathbf{k}'}\\ \hat{b}^{\dagger}_{-\mathbf{k}'}\end{pmatrix}^{T}\begin{pmatrix}M^{31}_{\mathbf{k}}M^{41}_{\mathbf{k}'} & M^{32}_{\mathbf{k}}M^{41}_{\mathbf{k}'} & M^{33}_{\mathbf{k}}M^{41}_{\mathbf{k}'} & M^{34}_{\mathbf{k}}M^{41}_{\mathbf{k}'}\\ M^{31}_{\mathbf{k}}M^{42}_{\mathbf{k}'} & M^{32}_{\mathbf{k}}M^{42}_{\mathbf{k}'} & M^{33}_{\mathbf{k}}M^{42}_{\mathbf{k}'} & M^{34}_{\mathbf{k}}M^{42}_{\mathbf{k}'}\\ M^{31}_{\mathbf{k}}M^{43}_{\mathbf{k}'} & M^{32}_{\mathbf{k}}M^{43}_{\mathbf{k}'} & M^{33}_{\mathbf{k}}M^{43}_{\mathbf{k}'} & M^{34}_{\mathbf{k}}M^{43}_{\mathbf{k}'}\\ M^{31}_{\mathbf{k}}M^{44}_{\mathbf{k}'} & M^{32}_{\mathbf{k}}M^{44}_{\mathbf{k}'} & M^{33}_{\mathbf{k}}M^{44}_{\mathbf{k}'} & M^{34}_{\mathbf{k}}M^{44}_{\mathbf{k}'}\end{pmatrix}\begin{pmatrix}\hat{a}_{\mathbf{k}}\\ \hat{a}^{\dagger}_{-\mathbf{k}}\\ \hat{b}_{\mathbf{k}}\\ \hat{b}^{\dagger}_{-\mathbf{k}}\end{pmatrix}, \tag{18}$$

which can easily be rewritten in a compact form by introducing a spinorlike object $\Psi(\mathbf{k}') = (a_{\mathbf{k}}\ a^{\dagger}_{-\mathbf{k}}\ b_{\mathbf{k}}\ b^{\dagger}_{-\mathbf{k}})^{T}$.

## V. IMPURITY IN THE MISCIBLE AND IMMISCIBLE PHASES

We now consider the impurity-condensate couplings—to both normal modes—at the linear level in $\hat{H}^{(1)}_{\text{imp-bos}}$ and at the bilinear level in $H^{(2)}_{\text{imp-bos}}$, as derived in the previous sections. We stress that bilinear terms, describing the scattering of the impurity off the condensate, are important for an accurate description of impurities in ultracold gases [34,35]. We now want to solve the full Hamiltonian:

$$\hat{H} = H_{\text{bos}} + H_{\text{imp}} + \hat{H}^{(1)}_{\text{imp-bos}} + H^{(2)}_{\text{imp-bos}}. \tag{19}$$

To do so, first we make use of a canonical transformation $\hat{S} = \exp(\mathrm{i}\hat{\mathbf{R}}\cdot\hat{\mathbf{P}}_A/\hbar)\exp(\mathrm{i}\hat{\mathbf{R}}\cdot\hat{\mathbf{P}}_B/\hbar)$ so the transformed Hamiltonian $\mathcal{H} = \hat{S}^{-1}\hat{H}\hat{S}$ describes the system in a frame of reference comoving with the impurity. Here $\hat{\mathbf{P}}_A = \sum_{\mathbf{k}}\ \hbar\mathbf{k}\ \hat{a}^{\dagger}_{\mathbf{k}}\hat{a}_{\mathbf{k}}$ and the similarly defined $\hat{\mathbf{P}}_B$ are the bosonic momenta in the $A$ and $B$ components, respectively, that we use as generators of spatial translations for bosons. We can now study the dynamics of the system by means of a time-dependent variational ansatz [10,34,36,37],

$$|\Psi(t)\rangle = e^{i\phi(t)}e^{\sum_{\mathbf{k}}\alpha_{\mathbf{k}}(t)a^{\dagger}_{\mathbf{k}}+\beta_{\mathbf{k}}(t)b^{\dagger}_{\mathbf{k}}-\text{H.c.}}|0\rangle^{A}_{\text{bos}}|0\rangle^{B}_{\text{bos}}, \tag{20}$$

where $|0\rangle^{i}_{\text{bos}}$ is the boson vacuum for the $i$ component. The coherent-state ansatz of Eq. (20) constitutes an exact solution for the ground state of an infinite-mass impurity. We subsequently numerically determine the variational coefficients $\alpha_{\mathbf{k}}(t)$, $\beta_{\mathbf{k}}(t)$ via the Euler-Lagrange equation obtained from the Lagrangian:

$$\mathscr{L} = \langle\Psi(t)|\mathrm{i}\hbar\partial_t - \hat{\mathcal{H}}|\Psi(t)\rangle. \tag{21}$$

The time evolution of the time-dependent phase $\phi(t)$, on the other hand, is found by projecting the Schrödinger equation onto the chosen variational wave function, i.e., by evaluating $\langle\Psi(t)|\mathrm{i}\hbar\partial_t|\Psi(t)\rangle = \langle\Psi(t)|\hat{\mathcal{H}}|\Psi(t)\rangle$ and numerically solving for $\phi(t)$. Finally, the dynamical overlap or Loschmidt echo,

$$S(t) = \langle\Psi(0)|e^{-\mathrm{i}\hat{\mathcal{H}}t/\hbar}|\Psi(0)\rangle = \langle\Psi(0)|\Psi(t)\rangle, \tag{22}$$

contains full information about the spectrum of the system, allowing one to immediately obtain the spectral function as

$$A(\omega) = 2\,\mathrm{Re}\int_0^{\infty} dt\ e^{\mathrm{i}\omega t}S(t), \tag{23}$$

which is immediately related to the Green's function $G$ via $A(\omega) = \mathrm{Im}\ G(\omega + \mathrm{i}0^{+})$, while also being experimentally accessible via radio-frequency spectroscopy [8].

As a concrete realization of this system, motivated by recent experiments [19,38,39], we consider a heteronuclear $^{41}$K - $^{87}$Rb Bose mixture—which we shall dub species 1 and 2, respectively—on top of which we consider a dilute third component realized with a different hyperfine state of $^{41}$K—dubbed I species. The atoms forming the bosonic reservoir are in their hyperfine ground state ($F = 1, m_F = 1$) for both species, while the $^{41}$K impurity is in the second-lowest hyperfine state ($F = 1, m_F = 0$); this specific configuration is not affected by spin-exchange collisions, which generally restrict the lifetime of atomic mixtures. In the impurity limit for the third component, the system is described by five scattering lengths, namely, $a_{\text{K-K}}$, $a_{\text{K-Rb}}$, $a_{\text{Rb-Rb}}$, $a_{\text{I-K}}$, $a_{\text{I-Rb}}$. Importantly, these scattering lengths are all known, and $a_{\text{K-Rb}}$ and $a_{\text{I-Rb}}$ can be tuned thanks to experimentally accessible Feshbach resonances [32,38,40–42]: In Fig. 1, we display the behavior of $a_{\text{K-Rb}}$ and $a_{\text{I-Rb}}$ as a function of the magnetic field $B$ in the range $B \in [60, 105]$ G. The other three scattering lengths are

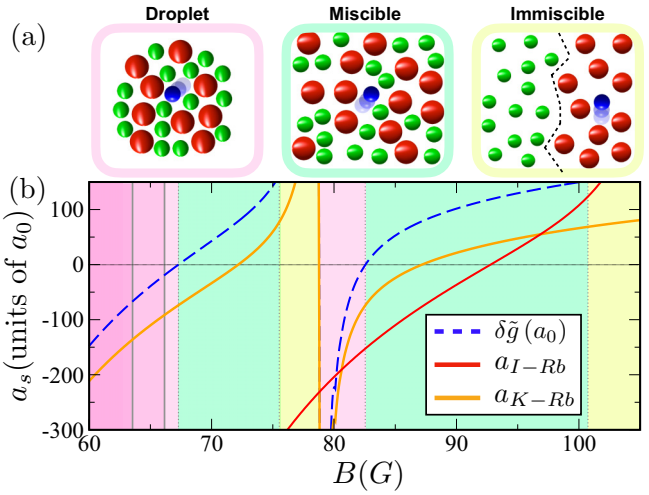


FIG. 1. Mobile impurity in a heteronuclear $^{87}$Rb - $^{41}$K mixture. (a) Quantum phases of the mixture. In the self-bound phase (pink region), the mixture forms a droplet, stabilized by quantum fluctuations, on which the impurity can reside. In the miscible phase (green region), the impurity lives in a bosonic mixture, whereas the yellow region corresponds to the immiscible, phase-separated regime, in which the impurity occupies the most energetically favorable of the two domains. (b) Tunable scattering lengths $a_{\text{I-Rb}}$ between the impurity and $^{87}$Rb (red) and the intercomponent scattering length $a_{\text{K-Rb}}$ (orange) across the magnetic field interval $B \in [60, 105]$ G; note the Feshbach resonance at $B = 78.9$ G. In this magnetic field range, $a_{\text{I-K}}$, $a_{\text{Rb-Rb}}$, and $a_{\text{K-K}}$ are approximately constant (see main text). Dashed blue: Effective scaled mean-field coupling $\delta\tilde{g} = \delta g\sqrt{m_1 m_2}/4\pi\hbar^2$ of the two-component mixture. When $\delta g < 0$, the system is unstable toward collapse and is stabilized by quantum fluctuations into a self-bound droplet phase (pink region). Full gray lines denote the transitions of impurities localized at the center (light pink), at the surface (pink) $63.5\,\text{G} < B < 66.1\,\text{G}$, or expelled from the droplet (dark pink) for $N_D = 4 \times 10^4$ particles in the droplet [see also Figs. 3(c)–3(f)].

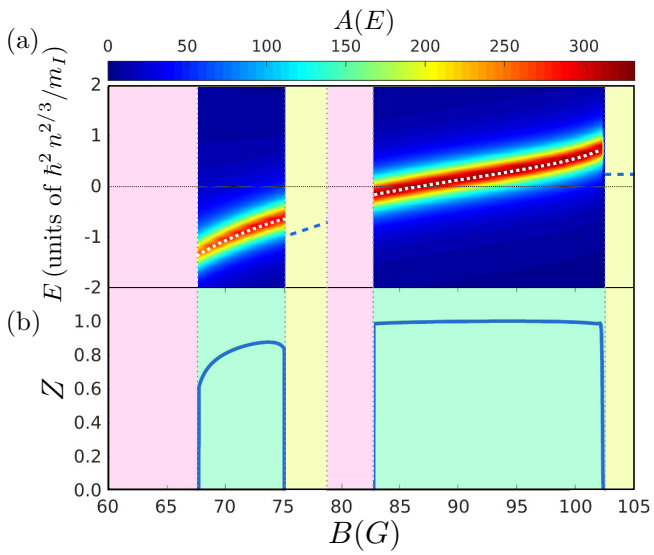


FIG. 2. Impurity properties in the miscible and immiscible phase. (a) Polaron spectral function $A(E)$ in the miscible phase of the mixture, as a function of external magnetic field $B$ and the polaron energy. The dotted white line shows the mean-field solution of the equations of motion, whereas the dashed blue line in the immiscible region shows the energy of the polaron coupled to a single component, see main text. Energies are scaled by the peak density $n$ of the mixture. (b) Quasiparticle weight $Z$ in the immiscible region, as a function of magnetic field $B$.

almost constant in the range considered, i.e., $a_{\text{K-K}} \simeq a_{\text{I-K}} \simeq 62\,a_0$, $a_{\text{Rb-Rb}} \simeq 100.4\,a_0$.

The liquid-gas transition parameter,

$$\delta g = g_{12} + \sqrt{g_{11} g_{22}}, \tag{24}$$

also shown in Fig. 1, allows us to chart the Bose mixture phase diagram: As the magnetic field is varied in the aforementioned range, the mixture goes through the droplet, miscible and immiscible phases. The main result of the present paper is the analysis of the fate of the impurity across this phase diagram.

In Fig. 2, we consider this heteronuclear Bose mixture and plot the impurity spectral function $A(E)$ as a function of the (scaled) energy $E$ and of the magnetic field $B$, aiming at studying the polaron in the miscible phase. In the whole range of magnetic field, both polaron couplings are off-resonant, so the many-body environment simply shifts the energy of a sharp quasiparticle peak—Fig. 2(a)—while maintaining a relatively large quasiparticle weight $Z$—Fig. 2(b). The quasiparticle weight is defined as $Z = |\langle\psi_0|\psi\rangle|^2$, where $|\psi_0\rangle$ is the wave function of a bare particle and $|\psi\rangle$ that of a dressed, i.e., interacting, quasiparticle [43]. We note that the energy of the quasiparticle peak is well approximated by the mean-field solution (dotted white line) obtained by setting $\dot{\alpha}_{\mathbf{k}}(t) = \dot{\beta}_{\mathbf{k}}(t) = 0$ in the equations of motion. In the same figure, we also characterize the immiscible phase polaron energy (dashed blue), considering that the polaron will reside in the most energetically favorable component.

## VI. IMPURITY IN A SELF-BOUND DROPLET

We now draw our attention to the droplet phase. Within the Gross-Pitaevskii (GP) formalism, the two BEC components are described by complex fields $\phi_i(\mathbf{r})$ with the associated energy functional

$$E_{bb}[\phi_i] = \int d^3r \sum_{i=1,2} \left( \frac{\hbar^2|\nabla\phi_i|^2}{2m_i} + \frac{g_{ii}}{2}|\phi_i|^4 \right) + g_{12}|\phi_1|^2|\phi_2|^2 + \frac{8}{15\pi^2\hbar^3} \times \left( m_1^{\frac{3}{5}} g_{11}|\phi_1|^2 + m_2^{\frac{3}{5}} g_{22}|\phi_2|^2 \right)^{\frac{5}{2}}, \tag{25}$$

where the last term is the beyond mean-field interaction for a general two-component mixture [44,45]. The impurity and interaction between the impurity and the Bose mixture are described by the energy functional

$$E_I = \int d^3r \frac{\hbar^2|\nabla\psi|^2}{2m_I} + (g_{ID}|\phi(\mathbf{r})|^2 + \mathscr{E}_{\text{BMF}}(\mathbf{r}))|\psi(\mathbf{r})|^2, \tag{26}$$

where now the impurity component is described by the wave function $\psi(\mathbf{r})$, the total density $n(\mathbf{r}) \equiv |\phi(\mathbf{r})|^2 = n_1(\mathbf{r}) + n_2(\mathbf{r})$, and $g_{ID}$ is an effective mean-field coupling

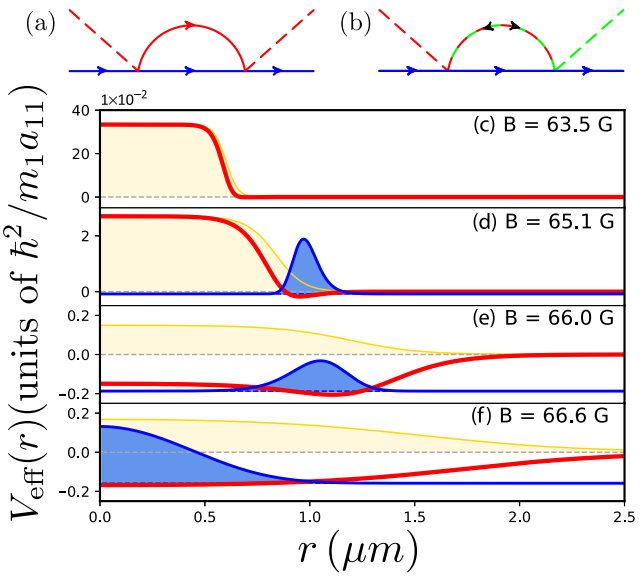


FIG. 3. Localized impurity in a self-bound droplet. (a), (b) Representative impurity-droplet Feynman diagrams at second-order perturbation theory in the small parameters $a_{Ii}/\xi_i$, $i = A, B$. The red and green dashed lines refer to the first and second normal modes of the condensate, respectively, each one being a different superposition of an excitation in the first and second components; the blue lines represent impurity propagators. (c)–(f) Effective impurity potential $V_{\rm eff}(r)$ (red curves) for an impurity in a self-bound droplet (yellow shaded region) with $N_D = 4 \times 10^4$. The impurity density (blue shaded) and its ground-state energy (blue dashed lines) are shown for several magnetic fields. (c) $B = 63.5$ G. The potential does not support bound states in three dimensions. (d) $B = 65.1$ G and (e) $B = 66.0$ G. The impurity is localized at the surface of the droplet at a distance $r \approx 1\mu$m from the center. (f) $B = 66.6$ G. The impurity is centered in the self-bound droplet.

constant (see Appendix A). The last term $\mathscr{E}_{\rm BMF}(\mathbf{r})$ is the beyond mean-field interaction for a general two-component mixture. We obtain it by means of perturbation theory in the small parameters $(a_{Ii}/\xi_i)$, $i = 1, 2$, where $\xi_i = 1/\sqrt{8\pi n_i a_{ii}}$ is the healing length for the $i$th component and $n_i$ is its density. This approach is equivalent to summing 16 different Feynman diagrams corresponding to second-order processes; some of the diagrams do not mix the normal modes of the condensate—as in Fig. 3(a) [46], whereas our binary mixture also allows for processes mixing the two normal modes, as in Fig. 3(b), each of the normal modes being a different superposition of the two original components in the condensate. We report here only the final results (see Appendix B). Within local-density approximation, one obtains

$$\mathscr{E}_{\rm BMF}(\mathbf{r}) = \left(\frac{2\pi\hbar^2\xi_1 n}{\mu_{I1}}\frac{1}{1+\alpha}\right)\left(\frac{a_{I1}}{\xi_1}\right)^2\frac{m_1}{\mu_{I1}}I_1 + \left(\frac{2\pi\hbar^2\xi_2 n}{\mu_{I2}}\frac{\alpha}{1+\alpha}\right)\left(\frac{a_{I2}}{\xi_2}\right)^2\frac{m_2}{\mu_{I2}}I_2, \quad (27)$$

where the total density $n(\mathbf{r})$ and the healing lengths $\xi_i(\mathbf{r})$ are evaluated at the impurity position and $I_i$, $i = 1, 2$ are dimensionless regularized integrals depending on the condensate Bogoliubov amplitudes, and the ratio $\alpha = \sqrt{g_{11}/g_{22}}$.

To probe the equilibrium properties of the impurity in a droplet environment, we set the relative number of particles in each of the two components to satisfy the constraint $N_1/N_2 = \sqrt{g_{22}/g_{11}}$ [14]. Rescaling lengths by $a_{11}$ and energies by $E_1 = \hbar^2/(m_1 a_{11}^2)$, we write a set of coupled generalized GP equations for the impurity-droplet system and we analyze the concrete case of the heteronuclear $^{41}$K-$^{87}$Rb mixture. In Figs. 3(c)–3(f) we report the radial density profiles for the condensate (yellow shaded region) and for the impurity (blue region) for four different values of the magnetic field. We also plot the effective potential exerted by the mixture on the impurity, $V_{\rm eff}(\mathbf{r}) = g_{ID}|\phi(\mathbf{r})|^2 + \mathscr{E}_{\rm BMF}(\mathbf{r})$, sum of the mean-field term proportional to $n(\mathbf{r})$, and $\mathscr{E}_{\rm BMF}(\mathbf{r})$ scaling as $n(\mathbf{r})^{3/2}$. The latter is repulsive, while the former can be attractive when $g_{ID} < 0$: In this case, occurring for our specific mixture, $V_{\rm eff}(\mathbf{r})$ is repulsive (attractive) in the high (low) density region of the droplet, giving rise to a rich phenomenology. For $B = 63.5$ G, in three dimensions $V_{\rm eff}(\mathbf{r})$ does not support bound states. As the magnetic field is increased, for $B = 65.1$ G and for $B = 66.0$ G we observe that the impurity is localized at the surface of the droplet [Fig. 4(b)]. Finally, as the magnetic field is further increased, we show that for $B = 66.6$ G the impurity is localized at the center of the self-bound droplet. Interestingly, these surface and center bound states occur in a range of magnetic fields where long-lived droplets have already been produced [19,39]. In current experiments, the existence of such states, in which the impurity either localizes at the center of the droplet or its surface, could be probed by performing high-resolution imaging [20]. Although we deal with the case of a single impurity, we expect that the results are not substantially affected for a small—but detectable—number of impurities, e.g., a few percent of the droplet atom number.

Finally, in Figs. 4(c)–4(e), we study excited states of the impurity. Depending on the magnetic field strengths, few bound states appear, their number depending also on the impurity angular momentum $\ell$. We notice that, for localized states at the surface, the lowest-energy impurity states of finite $\ell$ is well described by $E_I(\ell) = E_I(0) + \hbar^2\ell(\ell+1)/2m^*R^2$ [black dashed line in Fig. 4(e)], where $m^*$ is the effective mass and $R^{-2} = \langle r^{-2}\rangle$: the centrifugal barrier affects localized surface states at finite $\ell$, providing essentially a constant energy shift with respect to the $\ell = 0$ case (see Appendix C).

## VII. CONCLUSIONS AND OUTLOOK

We studied the effect of an impurity in a two-component heteronuclear Bose mixture. Focusing on collisionally stable, long-lived Bose mixtures of $^{41}$K - $^{87}$Rb, we discovered a nontrivial mechanism leading to the localization of the impurity in a droplet environment, based on a delicate balance between the mean-field attraction—scaling with $n_D(\mathbf{r})$—and repulsive quantum fluctuations—scaling with $n_D(\mathbf{r})^{3/2}$. This has far-reaching theoretical and experimental implications: Such impurity states, experimentally accessible by magnetic tuning, provide a tool for probing the droplet, whose study is currently hindered by the lack of adequate diagnostics. Similar to the case of doped helium droplets, one could unveil the droplet properties by spectroscopic measurements of the dopant impurities [47]: The detection by the local imagining of these polaronic states would permit the characterization of quantum

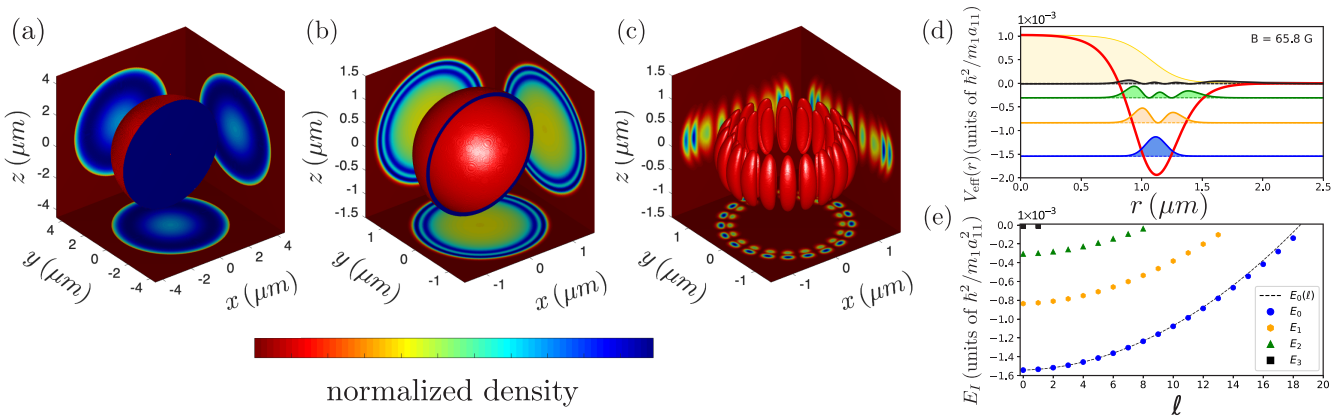


FIG. 4. Densities and excited states of the impurity. (a)–(c) Impurity density of the ground and excited states for $N_D = 4 \times 10^4$. Main figures: Isosurfaces of constant density. Planes display integrated densities along the axis orthogonal to the plane. Densities (color bar) are scaled by the maximum density of each configuration. (a) Ground state of an impurity centered in the droplet at $B = 66.6$ G. (b) Ground state of an impurity localized at the droplet surface at $B = 65.8$ G. (c) Excited state of an impurity at $B = 65.8$ G for $\ell = 10$ and $m = 10$. (d) Effective potential $V_{\rm eff}(r)$ and density of the impurity $n_I(r)$ for the $n = 0, \ldots, 3$ $s$-wave bound states for a spherical droplet with density $n_D(r)$ (yellow). The eigenstates are localized on the surface of the droplet at $r \approx 1.1$ $\mu$m from the droplet center. e) Spectrum of the impurity eigenstates in the presence of the effective potential $V_{\rm eff}$(r) of (a). The black dashed line is the analytical prediction $E_I(\ell) - E_I(0) \propto \ell(\ell+1)$ discussed in the text. Eigenstates with $n = 1$ and $\ell = 0$ and $\ell = 10$, $m = 10$ are shown in (b) and (c) respectively. The parameters for (d) and (e) are $N_D = 4 \times 10^4$ and $B = 65.8$ G.

fluctuations at the single-particle level of a complex many-body environment. Also, our setup would permit us to implement a scheme for the thermometry of the self-bound droplet: a weak quench of the magnetic field, $\Delta B \approx 1$ G, releases from the confining potential several bosonic impurities populating the lowest rovibronic states in thermal equilibrium with the droplet. Time-of-flight detection of the impurities would then permit the measurement of the temperature of the droplet.

Lastly, this study has far-reaching implications for further research, e.g., by considering a similar scenario with fermionic impurities [48], a finite Rabi coupling between the two BEC components [49,50], lower dimensionalities [50,51], the coupling to highly excited Rydberg states [52], heliophobic impurities residing on the surface of a $^4$He nanodroplet [47], or an impurity hybridizing rotational degrees of freedom with a bath [53–56].

## ACKNOWLEDGMENTS

We thank A. Simoni for providing the calculations of the intercomponent scattering lengths. We gratefully acknowledge stimulating discussions with L. A. Peña Ardila, R. Schmidt, H. Silva, V. Zampronio, and M. Prevedelli for careful reading. G.B. acknowledges support from the Austrian Science Fund (FWF) under Project No. M2641-N27. T.M. acknowledges CNPq for support through Bolsa de produtividade em Pesquisa No. 311079/2015-6. This work is supported by the Deutsche Forschungsgemeinschaft (DFG, German Research Foundation) under Germany's Excellence Strategy No. EXC2181/1-390900948 (the Heidelberg STRUCTURES Excellence Cluster). This work was supported by the Serrapilheira Institute (Grant No. Serra-1812-27802). We thank the High-Performance Computing Center (NPAD) at UFRN for providing computational resources.

## APPENDIX A: ENERGY FUNCTIONAL OF A HETERONUCLEAR SELF-BOUND DROPLET

To study the effect of an impurity in the droplet phase, we assume that the two components are described by a complex field $\phi_i(\mathbf{r})$ with the associated energy functional

$$E_{\rm bb} = \int d^3r \left( \sum_{i=1,2} \frac{\hbar^2 |\nabla\phi_i|^2}{2m_i} + \frac{g_{ii}}{2}|\phi_i|^4 \right) + g_{12}|\phi_1|^2|\phi_2|^2 + \frac{8}{15\pi^2\hbar^3}\left(m_1^{\frac{3}{5}} g_{11}|\phi_1|^2 + m_2^{\frac{3}{5}} g_{22}|\phi_2|^2\right)^{\frac{5}{2}}. \tag{A1}$$

The last term in Eq. (A1) is the beyond mean-field interaction for a general two-component mixture [44]. To probe the equilibrium properties, we set the relative number of particles in each of the two components to satisfy the constraint $\frac{N_1}{N_2} = \sqrt{\frac{g_{22}}{g_{11}}}$ [14]. Introducing the mass ratio $z = \frac{m_2}{m_1}$, the scaled mass $m^* = m\frac{1+\sqrt{z a_{11}/a_{22}}}{1+\sqrt{a_{11}/z a_{22}}}$, and the coupling constant ratio $\alpha = \sqrt{\frac{g_{11}}{g_{22}}} = z^{1/2}\sqrt{a_{11}/a_{22}}$ we can rewrite the densities of each component as follows

$$|\phi_1|^2 = \frac{1}{1+\alpha}|\phi|^2, \quad |\phi_2|^2 = \frac{\alpha}{1+\alpha}|\phi|^2, \tag{A2}$$

where $|\phi(\mathbf{r})|^2 = |\phi_1(\mathbf{r})|^2 + |\phi_2(\mathbf{r})|^2$. Using the definition $\delta g = g_{12} + \sqrt{g_{11}g_{22}}$ we can rewrite the energy functional

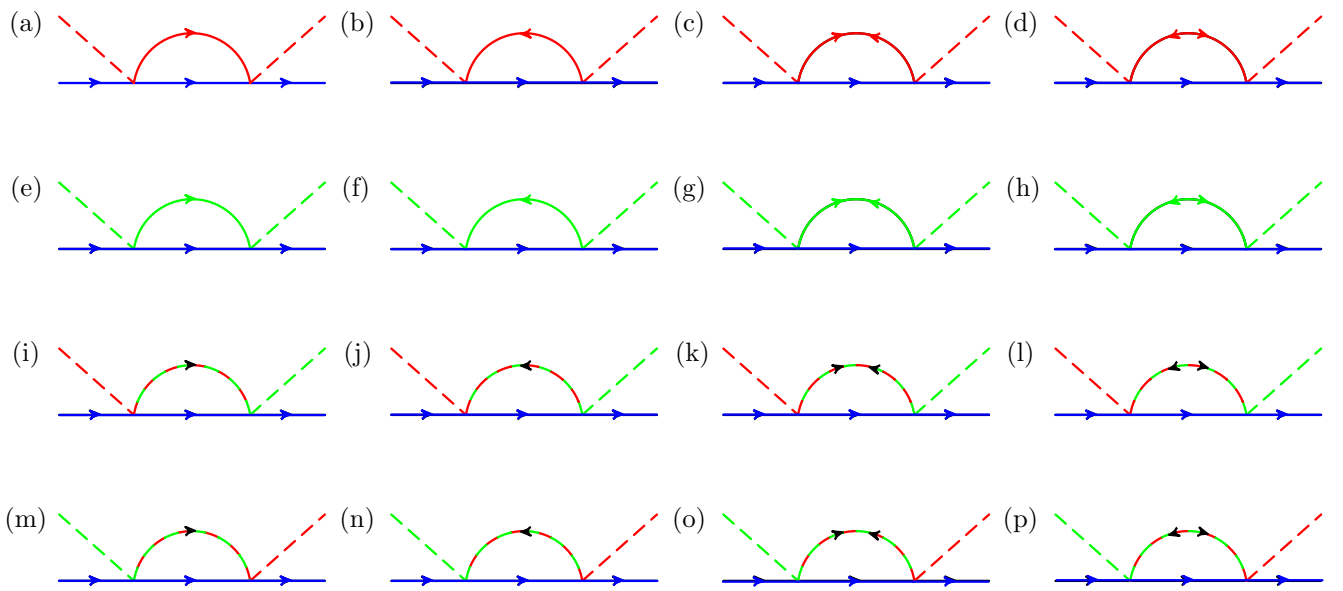


FIG. 5. Feynman diagrams of the interaction between the two-component BEC (red and green lines) and the impurity (blue lines). The arrows denote normal and anomalous propagators following the convention in Ref. [57].

$E_{\rm bb}$ as

$$E_{\rm bb}[\phi] = \int d^3r \frac{\hbar^2|\nabla\phi|^2}{2m^*} + \delta g \frac{\alpha}{(1+\alpha)^2}|\phi|^4 + \frac{8m_1^{\frac{3}{2}}}{15\pi^2\hbar^3}\left(\frac{g_{11}|\phi|^2}{1+\alpha}\right)^{\frac{5}{2}}\left(1+\frac{z^{\frac{3}{2}}}{\alpha^{\frac{1}{2}}}\right)^{\frac{5}{2}}. \quad \text{(A3)}$$

Scaling lengths by $a_{11}$ and energies by $E_1 = \frac{\hbar^2}{m_1 a_{11}^2}$, we can write a generalized GP equation for the self-bound droplet,

$$i\frac{\partial\phi}{\partial t} = \left(-\frac{\nabla^2}{2m^*/m_1} + g_{\rm MF}|\phi|^2 + g_{LHY}|\phi|^3\right)\phi(\mathbf{r},t), \quad \text{(A4)}$$

where we introduced the effective couplings:

$$\begin{cases} g_{\rm MF} &= 4\pi\frac{\alpha}{(1+\alpha)^2}\left(\frac{2}{\alpha}+\frac{a_{12}}{a_{11}}\frac{1+z}{z}\right) \\ g_{LHY} &= \frac{128\sqrt{\pi}}{3}\left(\frac{1+z^{\frac{1}{10}}\sqrt{a_{22}/a_{11}}}{1+\sqrt{z a_{11}/a_{22}}}\right)^{\frac{5}{2}}. \end{cases} \quad \text{(A5)}$$

We solve Eq. (A4) to obtain, e.g., the density profiles of Figs. 3 and 4(d) (yellow shaded areas). In Fig. 6, we plot the energy of the droplet as a function of the number of particles $N_D$ in the droplet [Fig. 6(a)] and as a function of the magnetic field $B$ [Fig. 6(b)].

## APPENDIX B: BEYOND-MEAN FIELD IMPURITY-BEC ENERGY $\mathscr{E}_{\rm BMF}(\mathbf{r})$

The mean-field impurity-droplet potential reads

$$V_{\rm eff}^{\rm mf}(\mathbf{r}) = |\phi(\mathbf{r})|^2\left(\frac{1}{1+\alpha}g_{I1} + \frac{\alpha}{1+\alpha}g_{I2}\right). \quad \text{(B1)}$$

Introducing the effective coupling,

$$g_{ID} = \frac{2\pi}{1+\alpha}\left(\frac{2a_{I1}}{a_{11}+\frac{\alpha a_{I2}}{a_{11}}\frac{1+z}{z}}\right), \quad \text{(B2)}$$

one obtains the first term of the impurity-droplet potential of Eq. (26) of the main text. We now compute the correction to the mean-field impurity-droplet energy in the perturbative limit for small $a_{Ii}/\xi_i$, $(i=1,2)$, where $\xi_i = 1/\sqrt{8\pi n_i a_{ii}}$ is the healing length of the $i$th component of the BEC. We focus on the second-order correction which can be derived using the generalized Fröhlich Hamiltonian derived in Sec. III. Within this approximation, the interaction Hamiltonian reads

$$\begin{aligned}\hat{H}_{\text{imp-bos}} &= \sqrt{n_1}\sum_{\mathbf{q},\mathbf{k}} V_A(\mathbf{q})\, e^{i\mathbf{q}\cdot\hat{\mathbf{R}}}\,(A_{\mathbf{q}} + A^\dagger_{-\mathbf{q}}) + \sqrt{n_2}\sum_{\mathbf{q},\mathbf{k}} V_B(\mathbf{q}) e^{i\mathbf{q}\cdot\hat{\mathbf{R}}}\,(B_{\mathbf{q}} + B^\dagger_{-\mathbf{q}}) \\ &= \sqrt{n_1}\sum_{\mathbf{q},\mathbf{k}} V_A(\mathbf{q})\, e^{i\mathbf{q}\cdot\hat{\mathbf{R}}}\big((M^{11}_{\mathbf{q}}+M^{21}_{\mathbf{q}})\hat{a}_{\mathbf{q}} + (M^{12}_{\mathbf{q}}+M^{22}_{\mathbf{q}})\hat{a}^\dagger_{-\mathbf{q}} + (M^{13}_{\mathbf{q}}+M^{23}_{\mathbf{q}})\hat{b}_{\mathbf{q}} + (M^{14}_{\mathbf{q}}+M^{24}_{\mathbf{q}})\hat{b}^\dagger_{-\mathbf{q}}\big) + \\ &+ \sqrt{n_2}\sum_{\mathbf{q},\mathbf{k}} V_B(\mathbf{q})\, e^{i\mathbf{q}\cdot\hat{\mathbf{R}}}\big((M^{31}_{\mathbf{q}}+M^{41}_{\mathbf{q}})\hat{a}_{\mathbf{q}} + (M^{32}_{\mathbf{q}}+M^{42}_{\mathbf{q}})\hat{a}^\dagger_{-\mathbf{q}} + (M^{33}_{\mathbf{q}}+M^{43}_{\mathbf{q}})\hat{b}_{\mathbf{q}} + (M^{34}_{\mathbf{q}}+M^{44}_{\mathbf{q}})\hat{b}^\dagger_{-\mathbf{q}}\big). \end{aligned} \quad \text{(B3)}$$

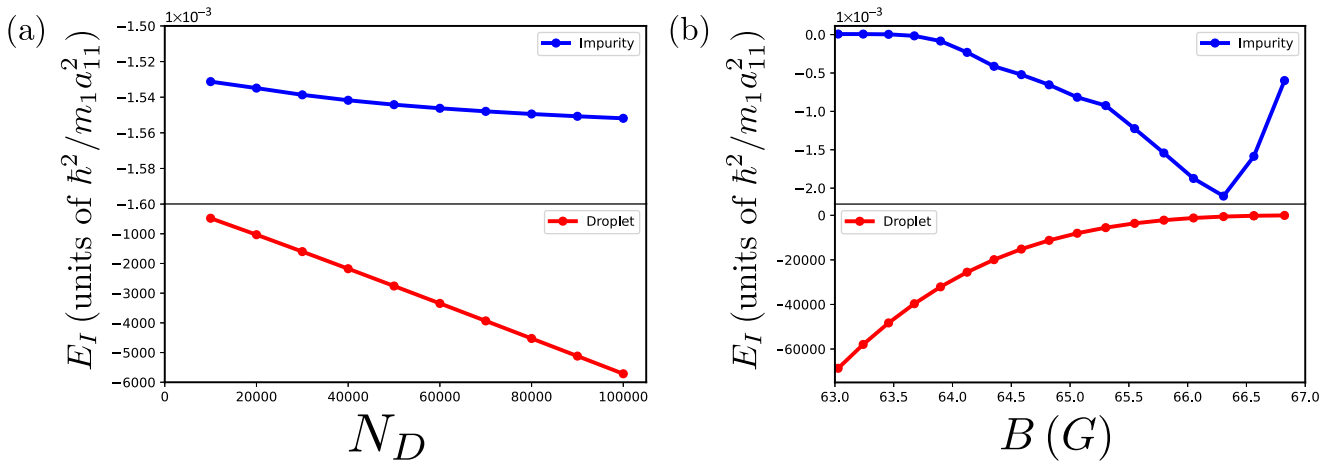


FIG. 6. Energies $E_I$ of the impurity (blue) and $E_D$ of the droplet (red) in units of $\hbar^2/m_1a_{11}^2$ as a function of (a) the number of particles in the droplet $N_D$ and (b) the magnetic field $B$ (G). In (a), we set $B = 65.8$ G and in (b) $N_D = 4 \times 10^4$.

We then apply perturbation theory to find the correction to the ground-state energy. The first-order correction $\Delta E^{(1)}$ vanishes. The second-order correction reads

$$\Delta E^{(2)} = n\frac{1}{1+\alpha}\left(\frac{2\pi\hbar^2 a_{1I}}{\mu_{1I}}\right)^2 \int \frac{d^3k}{(2\pi)^3}\left(-\frac{\left|\left(M_{\mathbf{k}}^{12}+M_{\mathbf{k}}^{22}\right)+\sqrt{\alpha}\frac{a_{2I}}{a_{1I}}\frac{\mu_{1I}}{\mu_{2I}}\left(M_{\mathbf{k}}^{32}+M_{\mathbf{k}}^{42}\right)\right|^2}{\omega_k^{(A)}}+\frac{2\mu_{1I}}{\hbar^2k^2}\right)$$
$$+ n\frac{\alpha}{1+\alpha}\left(\frac{2\pi\hbar^2 a_{2I}}{\mu_{2I}}\right)^2 \int \frac{d^3k}{(2\pi)^3}\left(-\frac{\left|\left(M_{\mathbf{k}}^{34}+M_{\mathbf{k}}^{44}\right)+\left(\sqrt{\alpha}\frac{a_{2I}}{a_{1I}}\frac{\mu_{1I}}{\mu_{2I}}\right)^{-1}\left(M_{\mathbf{k}}^{14}+M_{\mathbf{k}}^{24}\right)\right|^2}{\omega_k^{(B)}}+\frac{2\mu_{2I}}{\hbar^2k^2}\right). \tag{B4}$$

The last term in the two integrands acts as a regularizing term for the pair integrals and has the same form as in the Lippmann-Schwinger equation for each one of the two components. The second-order energy shift can be equivalently expressed as the sum of Feynman diagrams shown in Fig. 5.

Finally, Eq. (B4) can be recast as in Eq. (27) of the main text upon introducing the healing lengths of the each component $\xi_i = (8\pi n_i a_{ii})^{-1/2}$, $i = 1, 2$. With the help of the substitutions $\frac{\hbar^2k^2}{2m_i} = K^2 n_i \frac{4\pi\hbar^2 a_{ii}}{2m_i}$, $i = 1, 2$ we obtain

$$\mathscr{E}_{\rm BMF} = \frac{1}{1+\alpha}\left(\frac{2\pi\hbar^2\xi_1 n}{\mu_{I1}}\right)\left(\frac{a_{I1}}{\xi_1}\right)^2\frac{m_1}{\mu_{I1}}I_1 + \frac{\alpha}{1+\alpha}\left(\frac{2\pi\hbar^2\xi_2 n}{\mu_{I2}}\right)\left(\frac{a_{I2}}{\xi_2}\right)^2\frac{m_2}{\mu_{I2}}I_2, \tag{B5}$$

where we introduced the dimensionless integrals:

$$I_1 = \frac{2}{\pi}\int d^3K\left(-\frac{\left|\left(M_{\mathbf{K}}^{12}+M_{\mathbf{K}}^{22}\right)+\sqrt{\alpha}\frac{a_{2I}}{a_{1I}}\frac{\mu_{1I}}{\mu_{2I}}\left(M_{\mathbf{K}}^{32}+M_{\mathbf{K}}^{42}\right)\right|^2}{\omega_K^{(A)}}+\frac{\mu_{1I}}{m_1}\frac{1}{K^2}\right),$$
$$I_2 = \frac{2}{\pi}\int d^3K\left(-\frac{\left|\left(M_{\mathbf{K}}^{34}+M_{\mathbf{K}}^{44}\right)+\left(\sqrt{\alpha}\frac{a_{2I}}{a_{1I}}\frac{\mu_{1I}}{\mu_{2I}}\right)^{-1}\left(M_{\mathbf{K}}^{14}+M_{\mathbf{K}}^{24}\right)\right|^2}{\omega_K^{(B)}}+\frac{\mu_{2I}}{m_2}\frac{1}{K^2}\right). \tag{B6}$$

We employ local-density approximation to account for the space-dependent condensate profiles, leading to a *generalized* Lee-Huang-Yang type of beyond-mean field energy shift for the impurity. The sum of the contributions of Eqs. (B1) and (B5) concludes the derivation of the effective potential in Eq. (26) of the main text:

$$V_{\rm eff}(\mathbf{r}) = g_{ID}|\phi(\mathbf{r})|^2 + \mathscr{E}_{\rm BMF}(\mathbf{r}). \tag{B7}$$

Importantly, we notice that the mean-field correction is linear in the droplet density $n(\mathbf{r})$, whereas the beyond-mean-field contribution $\mathscr{E}_{\rm BMF}(\mathbf{r})$ scales as $n(\mathbf{r})^{3/2}$. In Fig. 6, we plot the energy of the impurity as a function of the number of particles in the droplet (a) and as a function of the magnetic field (b). We observe that the impurity energy is a nonmonotonic function of the magnetic field. Finally, we notice that, due to the large energy difference between the droplet and the

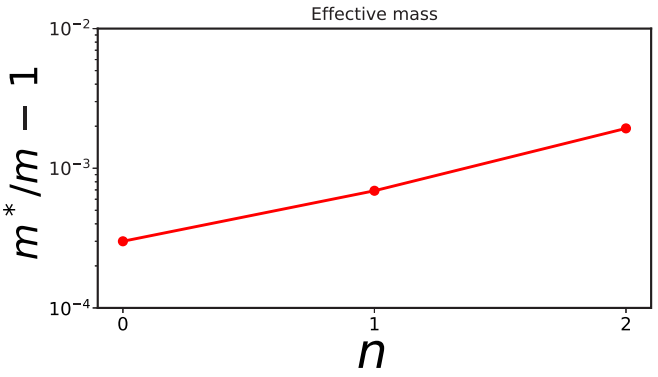


FIG. 7. Effective mass in the droplet phase. $m^*/m - 1$ for the first three vibrational states in Fig. 4(d).

impurity, we neglect the back action of the impurity on the droplet.

## APPENDIX C: EFFECTIVE MASS OF THE IMPURITY IN THE DROPLET PHASE

In the uniform phase, the polaron effective mass $m^*$ is expected to be very close to the impurity bare mass $m$ since the spectral weight $Z$ is very close to one. This means that the polaron is weakly dressed by the excitations of the mixture. Another confirmation of this observation comes from the relatively weak interaction between the impurity and the two-component BEC (see Fig. 1), even in presence of strong interactions in the mixture.

The estimate of the effective mass in the droplet phase is a more intriguing case. As the droplet is an inhomogeneous environment for the impurity, the effective mass $m^*$ cannot be straightforwardly extracted with the standard approach from the second derivative of the dispersion relation with respect to a small momentum shift of the polaron [58]. Instead, one could extract the effective mass by noting the analogy between the localized impurity and a three-dimensional quantum rotor (see Fig. 4) with both vibrational Fig. 4(d)] and rotational states [Fig. 4(e)]. The procedure we describe here is routinely applied to determine polaron effective masses of impurities in helium clusters (see, for instance, Ref. [47]). Vibrational and rotational states are discrete and labeled by quantum numbers $n$ and $\ell$ (orbital angular momentum), respectively. One can extract the effective mass of the impurity by fitting the rotational energies in Fig. 4(e) with the equation

$$E_n(\ell) = B_n\,\ell(\ell+1), \tag{C1}$$

and setting the rotation constant $B_n = \frac{\hbar^2}{2m^* R_n^2}$. The radius $R_n^{-2} = \langle r^{-2}\rangle_n$ is determined from the expectation value in the $n$th vibrational state. The results are shown in Fig. 7 for the first three vibrational states.


[1] J. T. Devreese, Polarons, Encycl. Appl.. Phys. **14**, 383 (1996).
[2] L. D. Landau, Phys. Z. Sowjetunion **3**, 664 (1933).
[3] L. Landau and S. Pekar, Effective mass of a polaron, Zh. Eksp. Teor. Fiz **18**, 419 (1948).
[4] H. Fröhlich, Electrons in lattice fields, Adv. Phys. **3**, 325 (1954).
[5] R. P. Feynman, Slow electrons in a polar crystal, Phys. Rev. **97**, 660 (1955).
[6] F. Grusdt and E. Demler, New theoretical approaches to Bose polarons, in *Proceedings of the International School of Physics "Enrico Fermi," Quantum Matter at Ultralow Temperatures*, edited by M. Inguscio, W. Ketterle, S. Stringari, and G. Roati (IOS Press, Amsterdam, 2015), Vol. 191, pp. 325–411.
[7] M.-G. Hu, M. J. Van de Graaff, D. Kedar, J. P. Corson, E. A. Cornell, and D. S. Jin, Bose Polarons in the Strongly Interacting Regime, Phys. Rev. Lett. **117**, 055301 (2016).
[8] N. B. Jørgensen, L. Wacker, K. T. Skalmstang, M. M. Parish, J. Levinsen, R. S. Christensen, G. M. Bruun, and J. J. Arlt, Observation of Attractive and Repulsive Polarons in a Bose-Einstein Condensate, Phys. Rev. Lett. **117**, 055302 (2016).
[9] E. Compagno, G. De Chiara, D. G. Angelakis, and G. M. Palma, Tunable polarons in Bose-Einstein condensates, Sci. Rep. **7**, 2355 (2017).
[10] Y. Ashida, R. Schmidt, L. Tarruell, and E. Demler, Many-body interferometry of magnetic polaron dynamics, Phys. Rev. B **97**, 060302(R) (2018).
[11] A. Boudjemâa, N. Guebli, M. Sekmane, and S. Khlifa-Karfa, Breathing modes of repulsive polarons in Bose–Bose mixtures, J. Phys.: Condens. Matter **32**, 415401 (2020).
[12] F. Kh. Abdullaev and R. M. Galimzyanov, Bosonic impurity in a one-dimensional quantum droplet in the BoseBose mixture, J. Phys. B: At. Mol. Opt. Phys. **53**, 165301 (2020).
[13] K. Keiler, S. I. Mistakidis, and P. Schmelcher, Polarons and their induced interactions in highly imbalanced triple mixtures, Phys. Rev. A **104**, L031301 (2021).
[14] D. S. Petrov, Quantum Mechanical Stabilization of a Collapsing Bose-Bose Mixture, Phys. Rev. Lett. **115**, 155302 (2015).
[15] D. S. Petrov and G. E. Astrakharchik, Ultradilute Low-Dimensional Liquids, Phys. Rev. Lett. **117**, 100401 (2016).
[16] C. R. Cabrera, L. Tanzi, J. Sanz, B. Naylor, P. Thomas, P. Cheiney, and L. Tarrue, Quantum liquid droplets in a mixture of Bose-Einstein condensates, Science **359**, 301 (2018).
[17] P. Cheiney, C. R. Cabrera, J. Sanz, B. Naylor, L. Tanzi, and L. Tarruell, Bright Soliton to Quantum Droplet Transition in a Mixture of Bose-Einstein Condensates, Phys. Rev. Lett. **120**, 135301 (2018).
[18] G. Semeghini, G. Ferioli, L. Masi, C. Mazzinghi, L. Wolswijk, F. Minardi, M. Modugno, G. Modugno, M. Inguscio, and M. Fattori, Self-Bound Quantum Droplets of Atomic Mixtures in Free Space, Phys. Rev. Lett. **120**, 235301 (2018).
[19] C. D'Errico, A. Burchianti, M. Prevedelli, L. Salasnich, F. Ancilotto, M. Modugno, F. Minardi, and C. Fort, Observation of quantum droplets in a heteronuclear bosonic mixture, Phys. Rev. Research **1**, 033155 (2019).
[20] Z. Guo, F. Jia, L. Li, Y. Ma, J. M. Hutson, X. Cui, and D. Wang, Lee-Huang-Yang effects in the ultracold mixture of $^{23}$Na and $^{87}$Rb with attractive interspecies interactions, Phys. Rev. Research **3**, 033247 (2021).
[21] N. Defenu, T. Donner, T. Macrì, G. Pagano, S. Ruffo and A. Trombettoni, Long-range interacting quantum systems, arXiv:2109.01063.

[22] H. Kadau, M. Schmitt, M. Wenzel, C. Wink, T. Maier, I. Ferrier-Barbut, and T. Pfau, Observing the Rosensweig instability of a quantum ferrofluid, Nature (London) **530**, 194 (2016).
[23] I. Ferrier-Barbut, H. Kadau, M. Schmitt, M. Wenzel, and T. Pfau, Observation of Quantum Droplets in a Strongly Dipolar Bose Gas, Phys. Rev. Lett. **116**, 215301 (2016).
[24] M. Schmitt, M. Wenzel, F. Böttcher, I. Ferrier-Barbut, and T. Pfau, Self-bound droplets of a dilute magnetic quantum liquid, Nature (London) **539**, 259 (2016).
[25] L. Chomaz, S. Baier, D. Petter, M. J. Mark, F. Wächtler, L. Santos, and F. Ferlaino, Quantum-Fluctuation-Driven Crossover from a Dilute Bose-Einstein Condensate to a Macrodroplet in a Dipolar Quantum Fluid, Phys. Rev. X **6**, 041039 (2016).
[26] I. Ferrier-Barbut, M. Schmitt, M. Wenzel, H. Kadau, and T. Pfau, Liquid quantum droplets of ultracold magnetic atoms, J. Phys. B: At. Mol. Opt. Phys. **49**, 214004 (2016).
[27] M. Wenzel, F. Böttcher, T. Langen, I. Ferrier-Barbut, and T. Pfau, Striped states in a many-body system of tilted dipoles, Phys. Rev. A **96**, 053630 (2017).
[28] A. Boudjemâa, Fluctuations and quantum self-bound droplets in a dipolar Bose-Bose mixture, Phys. Rev. A **98**, 033612 (2018).
[29] J. C. Smith, D. Baillie, and P. B. Blakie, Quantum Droplet States of a Binary Magnetic Gas, Phys. Rev. Lett. **126**, 025302 (2021).
[30] R. N. Bisset, L. A. Pena Ardila, and L. Santos, Quantum Droplets of Dipolar Mixtures, Phys. Rev. Lett. **126**, 025301 (2021).
[31] A.-C. Lee, D. Baillie, P. B. Blakie, and R. N. Bisset, Miscibility and stability of dipolar bosonic mixtures, Phys. Rev. A **103**, 063301 (2021).
[32] G. Thalhammer, G. Barontini, L. De Sarlo, J. Catani, F. Minardi, and M. Inguscio, Double Species Bose-Einstein Condensate with Tunable Interspecies Interactions, Phys. Rev. Lett. **100**, 210402 (2008).
[33] D. M. Larsen, Binary mixtures of dilute Bose gases with repulsive interactions at low temperature, Ann. Phys. **24**, 89 (1963).
[34] Y. E. Shchadilova, R. Schmidt, F. Grusdt, and E. Demler, Quantum Dynamics of Ultracold Bose Polarons, Phys. Rev. Lett. **117**, 113002 (2016).
[35] S. P. Rath and R. Schmidt, Field-theoretical study of the Bose polaron, Phys. Rev. A **88**, 053632 (2013).
[36] P. Kramer and M. Saraceno, *Geometry of the Time-Dependent Variational Principle in Quantum Mechanics* (Springer-Verlag, Berlin, 1981).
[37] L. A. Pena Ardila, Dynamical formation of polarons in a Bose-Einstein condensate: A variational approach, Phys. Rev. A **103**, 033323 (2021).
[38] G. Thalhammer, G. Barontini, J. Catani, F. Rabatti, C. Weber, A. Simoni, F. Minardi, and M. Inguscio, Collisional and molecular spectroscopy in an ultracold Bose-Bose mixture, New J. Phys. **11**, 055044 (2009).
[39] A. Burchianti, C. D'Errico, M. Prevedelli, L. Salasnich, F. Ancilotto, M. Modugno, F. Minardi, and C. Fort, A dual-species Bose-Einstein condensate with attractive interspecies interactions, Condensed Matter **5**, 21 (2020).
[40] F. Ferlaino, C. D'Errico, G. Roati, M. Zaccanti, M. Inguscio, G. Modugno, and A. Simoni, Feshbach spectroscopy of a K-Rb atomic mixture, Phys. Rev. A **73**, 040702(R) (2006).
[41] C. D'Errico, M. Zaccanti, M. Fattori, G. Roati, M. Inguscio, G. Modugno, and A. Simoni, Feshbach resonances in ultracold 39 K, New J. Phys. **9**, 223 (2007).
[42] A. Simoni, M. Zaccanti, C. D'Errico, M. Fattori, G. Roati, M. Inguscio, and G. Modugno, Near-threshold model for ultracold KRb dimers from interisotope Feshbach spectroscopy, Phys. Rev. A **77**, 052705 (2008).
[43] P. Coleman, *Introduction to Many Body Physics* (Cambridge University Press, 2015).
[44] F. Minardi, F. Ancilotto, A. Burchianti, C. D'Errico, C. Fort, and M. Modugno, Effective expression of the Lee-Huang-Yang energy functional for heteronuclear mixtures, Phys. Rev. A **100**, 063636 (2019).
[45] P. Naidon and D. S. Petrov, Mixed Bubbles in Bose-Bose Mixtures, Phys. Rev. Lett. **126**, 115301 (2021).
[46] R. S. Christensen, J. Levinsen, and G. M. Bruun, Quasiparticle Properties of a Mobile Impurity in a Bose-Einstein Condensate, Phys. Rev. Lett. **115**, 160401 (2015).
[47] J.P. Toennies, and A.F. Vilesov, Superfluid helium droplets: A uniquely cold nanomatrix for molecules and molecular complexes, Angew. Chem., Int. Ed. **43**, 2622 (2004).
[48] M. Wenzel, T. Pfau, and I. Ferrier-Barbut, A fermionic impurity in a dipolar quantum droplet, Phys. Scr. **93**, 104004 (2018).
[49] A. Cappellaro, T. Macrì, G. F. Bertacco, and L. Salasnich, Equation of state and self-bound droplet in Rabi-coupled Bose mixtures, Sci. Rep. **7**, 13358 (2017).
[50] C. Charalambous, M. Á. García-March, G. Muñoz-Gil, P. R. Grzybowski, and M. Lewenstein, Control of anomalous diffusion of a Bose polaron, Quantum **4**, 232 (2020).
[51] S. I. Mistakidis, T. Mithun, P. G. Kevrekidis, H. R. Sadeghpour, and P. Schmelcher, Formation and quench of homo- and hetero-nuclear quantum droplets in one-dimension, Phys. Rev. Research **3**, 043128 (2021).
[52] R. Schmidt, H. R. Sadeghpour, and E. Demler, Mesoscopic Rydberg Impurity in an Atomic Quantum Gas, Phys. Rev. Lett. **116**, 105302 (2016).
[53] X. Li, G. Bighin, E. Yakaboylu, M. Lemeshko, Variational approaches to quantum impurities: From the Frhlich polaron to the angulon, Mol. Phys. **117**, 1981 (2019).
[54] X. Li, E. Yakaboylu, G. Bighin, R. Schmidt, M. Lemeshko, A. Deuchert, Intermolecular forces and correlations mediated by a phonon bath, J. Chem. Phys. **152**, 164302 (2020).
[55] M. Lemeshko, Quasiparticle Approach to Molecules Interacting with Quantum Solvents, Phys. Rev. Lett. **118**, 095301 (2017).
[56] G. Bighin and M. Lemeshko, Diagrammatic approach to orbital quantum impurities interacting with a many-particle environment, Phys. Rev. B **96**, 085410 (2017).
[57] A. L. Fetter and J. D. Walecka, *Quantum Theory of Many Particle Systems* (McGraw-Hill, New York, 1971).
[58] C. Kittel, *Introduction to Solid State Physics* (Wiley, New York, 2005).